

Optical microvariability of EGRET blazars^{*}

Gustavo E. Romero^{1, **}, Sergio A. Cellone², Jorge A. Combi^{1, **}, Ileana Andruchow¹

¹ Instituto Argentino de Radioastronomía, C.C.5, (1894) Villa Elisa, Buenos Aires, Argentina

² Facultad de Ciencias Astronómicas y Geofísicas, UNLP, Paseo del Bosque, 1900 La Plata, Buenos Aires, Argentina

Received 15 January 2002 / Accepted 15 May 2002

Abstract. We present results of a photometric CCD study of the incidence of microvariability in the optical emission of a sample of 20 blazars detected at gamma-ray energies by the EGRET instrument of the Compton Gamma-Ray Observatory. We have observed strong outbursts in some sources, but many others displayed no significant variability on timescales of hours. The typical minimum timescale results to be of \sim several hours, not tens of minutes as claimed by some authors. The duty cycle for optical intranight microvariations of gamma-ray blazars, as estimated from our observations, seems to be \sim 50 %, lower than what is usually assumed. For night-to-night variations, instead, the duty cycle approaches to what is observed in radio-selected BL Lacs and flat-spectrum radio quasars (i.e. \sim 70 %).

Key words. galaxies: active – galaxies: photometry – BL Lacertae objects: general – gamma-rays: observations

1. Introduction

The rapid changes in the optical brightness of blazars, typically with timescales of less than a single night, are well known. The existence of this phenomenon, usually called *microvariability*, was only accepted by the astronomical community after the advent of modern CCD photometry in the 1980s (Miller et al. 1989), despite the existence of previous reports (e.g., Racine 1970). In its most extreme manifestations the microvariations of blazars can reach values of more than 100% in less than 24 hours (e.g., Romero et al. 2000a). The origin of such an amazing behaviour is yet not clear.

The duty cycles (i.e., the fraction of time spent by a given source or group of sources displaying microfluctuations) for different classes of AGNs are not well known, but is usually thought that in radio-loud quasars (RLQs) and radio-selected BL Lac objects (RBLs) they are higher than those presented by X-ray selected BL Lacs (XBLs) and radio-quiet quasars (RQQs) (e.g., Heidt & Wagner 1996, 1998; Romero et al. 1999; Gopal-Krishna et al. 2000; Qian, Tao, & Fan 2000, 2002). Duty cycles of RBLs and RLQs are estimated to be \sim 70%, whereas the corresponding values for XBLs and RQQs seem to be \sim 30% and \sim 7%, re-

spectively (Romero et al. 1999). The high optical duty cycles displayed by strong flat-spectrum radio sources seem to be a consequence of the presence of relativistic jets oriented close to the line of sight in these objects. The microfluctuations could arise from interactions of relativistic shocks with small features in the parsec-scale jets (e.g., Qian et al. 1991, 2000; Romero 1995; Kraus et al. 1999). The lower duty cycles of XBLs could be a consequence of the stronger magnetic fields in these objects (e.g., Romero et al. 1999). In RQQs, the microvariations are possibly related to instabilities and orbiting hot spots in the accretion disks (e.g., Mangalam & Wiita 1993), and the duty cycles are perhaps reflecting the incidence of these phenomena in the innermost part of the disks.

If the scenario outlined above is basically correct, one could expect that gamma-ray blazars, the most energetic subclass of RL objects, should present the highest duty cycles of all AGNs. In fact, some recent monitoring campaigns by Xie et al. (1999, 2001, 2002) seem to suggest high duty cycles in a sample of northern blazars that have been detected by the Energetic Gamma Ray Experiment Telescope (EGRET) of the late Compton Gamma-Ray Observatory. However, comparison with duty cycles presented by other classes of objects requires uniform procedures for data analysis and error control. Very recently, Cellone et al. (2000) have demonstrated through a combination of observations and photometric simulations that small seeing fluctuations can be an important source of spurious microfluctuations in differential photometry due to variable contamination by light from host galaxies.

Send offprint requests to: Gustavo E. Romero

^{*} Based on observations made at the Complejo Astronómico El Leoncito, which is operated under agreement between CONICET and the National Universities of La Plata, Córdoba, and San Juan.

^{**} Member of CONICET

Comparison of results obtained by differential photometry with different instruments and different photometric apertures should be treated with extreme care. Some recent contradictory claims in microvariability research could be due to an incorrect treatment of the errors in this kind of observations (see Cellone et al. 2000, for a detailed discussion).

In this paper we present results of an extensive study of the incidence of microvariability in a sample formed mostly by southern gamma-ray blazars. Observational technique and error control follow the guidelines given by Cellone et al. (2000) and, consequently, our results can be compared with those obtained by Romero et al. (1999) for other types of AGNs, since both studies were conducted with the same instrument and identical procedures for data analysis.

In the next section we shall present our sample and describe the observations and the data analysis. We then present our main results in Sect. 3. The duty cycle for EGRET blazars is estimated in Sect. 4 and compared with other results found in the literature. We close in Sect. 5 with a brief discussion on the origin of microvariability in blazars.

2. Observations and data analysis

The Third EGRET Catalog (Hartman et al. 1999) lists 271 point-like gamma-ray sources. Of these sources 66 have been positively identified with blazars, which are usually strong flat-spectrum radio sources (e.g., Mattox et al. 1997). We have selected a sample of 20 of these blazars that satisfy the following criteria: 1) they are located at declinations lower than $+20^\circ$, and 2) they are brighter than magnitude $m_V = 19.0$. All these sources fall within the categories of RBLs, XBL or RLQs, where we include both highly polarized QSOs (HPQs) and optically variable violent QSOs (OVVQs). The sample is presented in Table 1, where we list, from left to right, the name of the object, the coordinates (RA and DEC) at J2000.0, the redshift, the magnitude in the V band, the object type, the name of the corresponding source in the Third EGRET Catalog, the averaged gamma-ray flux in units of 10^{-8} ph cm $^{-2}$ s $^{-1}$, its error, and the high-energy photon spectral index Γ .

Objects of this sample were monitored repeatedly during several observing sessions with the 2.15-m CASLEO telescope at El Leoncito, San Juan, Argentina, from July 1997 till July 2001. The instrument was equipped with a liquid-nitrogen-cooled CCD camera, using a Tek-1024 chip with a read-out-noise of 9.6 electrons and a gain of 1.98 electrons adu $^{-1}$. This is the same camera used by Romero et al. (1999) for a comparative study of duty cycles of radio-loud and radio-quiet QSOs. The unvignetted field was approximately 9 arcminutes in diameter, and consequently large enough as to contain several stars for comparison and variability control. Exposures varied from ~ 1 minute to ~ 5 minutes, according to the brightness of the object and the observing conditions. The quality of each night is coded with a parameter q , according to the follow-

ing scheme: photometric ($q = 1$), clear but seeing not very good ($q = 2$), thin cirrus ($q = 3$), thick cirrus or partially cloudy ($q = 4$). This information is given in column 3 of Table 2. It can be seen that 2/3 of our nightly lightcurves were obtained under good to very good atmospheric conditions.

The observations were made with a Johnson V filter. The CCD frames were bias-subtracted and flat-fielded using median-averaged dome flats, which resulted in a flat-field accuracy typically better than $\sim 0.5 - 1.0\%$ of the sky level. Standard stars from Landolt's (1992) fields were also observed each night for calibration to the standard system.

The data reduction was made with IRAF¹ software package running on a Linux workstation. Differential photometry was then made with the aperture routine APHOT. Each set of data for each object was always reduced with the same aperture radius, which was determined taking into account the apparent size and brightness of the host galaxy, in accordance with the recommendations by Cellone et al. (2000). The presence of neighbour stars was also taken into account, and in a few cases they had to be subtracted using DAOPHOT before performing aperture photometry. In any case, the aperture diameter was never lower than ~ 2.5 times the seeing FWHM.

Cross-checked non-variable stars in the field (with apparent magnitudes as close as possible to that of the target object) were divided in two groups, averaged, and used for comparison and control as in Romero et al. (1999). Differential lightcurves were then computed as target minus averaged comparison. In addition to the pure photometric errors, spurious variability was pondered through the scatter of the comparison minus control stars. The errors during a typical microvariability session (1 night) were mostly in the range $\sim 0.002 - 0.008$ mag, although in some particular cases they reached values of ~ 0.01 mag. Coordinates and magnitudes for the comparison ($C_{1,i}$) and control ($C_{2,i}$) stars in each AGN field are given in Table 3. Coordinates are accurate to ± 3 arcsec, while the accuracy of magnitudes varies between 0.05 and 0.10 mag, according to the photometric quality of each night. Hence, these data are given just to allow the identification of these stars by future observers, and should be used neither for astrometric purposes nor for photometric calibration to the standard system.

The variability criterion adopted in the present work is the 99%-confidence criterion used by Jang & Miller (1997), Romero et al. (1999), and many others: a parameter $C = \sigma_T/\sigma$ is introduced, where σ is the standard deviation of the control lightcurve and σ_T the deviation of the target differential lightcurve. A source can be then considered as variable at a 99% confidence if $C \geq 2.576$.

¹ IRAF is distributed by the National Optical Astronomy Observatories, which are operated by the Association of Universities for Research in Astronomy, Inc., under cooperative agreement with the National Science Foundation.

Table 1. Sample. The EGRET averaged (P1234) flux F is in units of 10^{-8} ph cm $^{-2}$ s $^{-1}$.

Object	$\alpha_{2000.0}$ hs min s	$\delta_{2000.0}$ ° ' "	z	m_V	Type	EGRET Name 3EG	F	ΔF	$\Gamma \pm \Delta\Gamma$
0208–512	02 10 46.2	–51 01 02	1.003	16.9	RLQ	J0210–5055	85.5	4.5	1.99 ± 0.05
0235+164	02 38 38.9	+16 36 59	0.904	19.0	RBL	J0237+1635	25.9	3.7	1.85 ± 0.12
0521–365	05 22 58.0	–36 27 31	0.055	14.5	RBL	J0536–3626	15.8	3.5	2.63 ± 0.42
0537–441	05 38 50.4	–44 05 09	0.894	15.5	RBL	J0540–4402	25.3	3.1	2.41 ± 0.12
1226+023	12 29 06.7	+02 03 09	0.158	12.8	RLQ	J1229+0210	15.4	1.8	2.58 ± 0.09
1229–021	12 32 00.0	–02 24 05	1.045	17.7	RLQ	J1230–0247	6.9	1.5	2.85 ± 0.30
1243–072	12 46 04.2	–07 30 47	1.286	19.0	RLQ	J1246–0651	9.8	2.1	2.73 ± 0.17
1253–055	12 56 11.2	–05 47 22	0.538	17.8	RLQ	J1255–0549	74.2	2.8	1.96 ± 0.04
1331+170	13 33 35.8	+16 49 04	2.084	16.7	RLQ	J1329+1708	4.4	1.6	2.41 ± 0.47
1334–127	13 37 39.8	–12 57 25	0.539	17.2	RLQ	J1339–1419	5.5	1.9	2.62 ± 0.42
1424–418	14 27 56.3	–42 06 19	1.522	17.7	RLQ	J1429–4217	11.9	2.7	2.13 ± 0.21
1510–089	15 12 50.3	–09 06 00	0.361	16.5	RLQ	J1512–0849	18.0	3.8	2.47 ± 0.21
1606+106	16 08 46.2	+10 29 08	1.226	18.5	RLQ	J1608+1055	25.0	4.5	2.63 ± 0.24
1622–297	16 26 06.0	–29 51 27	0.815	20.5	RLQ	J1625–2955	47.4	3.7	2.07 ± 0.07
1741–038	17 43 59.0	–03 50 05	1.054	18.6	RLQ	J1744–0310	11.7	3.3	2.42 ± 0.42
1933–400	19 37 16.2	–39 58 02	0.966	18.0	RLQ	J1935–4022	8.5	2.7	2.86 ± 0.40
2022–077	20 25 40.6	–07 35 52	1.388	18.5	RLQ	J2023–0836	21.2	3.5	2.38 ± 0.17
2155–304	21 58 52.1	–30 13 32	0.116	13.1	XBL	J2158–3023	13.2	3.2	2.35 ± 0.26
2230+114	22 32 36.4	+11 43 51	1.037	17.3	RLQ	J2233+1140	19.2	2.8	2.45 ± 0.14
2320–035	23 23 32.0	–03 17 05	1.411	18.6	RLQ	J2321–0328	< 6.0

3. Main results

The results of our observations are shown in Table 2, where we display, from left to right, the object name, the (Universal Time) date of the observations, the quality parameter of each night (see Sect. 2), the error determined from the standard deviation of the comparison lightcurve, the duration of each observing session, the classification of the source as variable (V) or non-variable (NV) according to the scheme explained in the previous section, the maximum magnitude fluctuation exhibited by the source in the course of a single night, and, finally, the average V magnitude (in the standard system) for each night of observations. This last parameter can be very different from what is listed in catalogs (see, for instance, Table 1), since it changes with time. Actually, it is clear that some sources that classify as NV at microvariability timescales can be variable from night to night (i.e., at *internight* timescales). Average magnitudes for nights with quality parameter $q = 3 - 4$ are probably affected by relatively high systematic errors ($\lesssim 0.5$ mag) and hence should be taken with care.

The most variable sources of our sample are the RBL objects AO 0235+164 and PKS 0537–441. We have communicated separately on the outbursts observed on November 1999 and December 1998, respectively, in these sources (Romero et al. 2000a,b). New data, from other observing sessions, are added in this paper. Anyway, the duty cycle of AO 0235+164 seems to be close to 1. On the contrary, PKS 0537–441 seems to switch between states with high-level of variability and quiet states. The intranight duty cycle for this source is $\sim 58.2\%$ (the *internight* value is about 81.6%). Many other gamma-ray blazars were ob-

served not to vary at all. For instance, the RLQ 1510–089 was monitored on 4 epochs during 1998 and 1999 and was always found NV at intranight timescales, although it was ~ 0.3 mag brighter in 1999. In Figures 1 and 2 we show, just as examples, two lightcurves: one for a variable source (0208–512, on the night of November 3rd, 1999, with $C = 18.01$) and one for a non-variable source (the usually considered ultra-variable RBL PKS 0537–441, on the night of December 22nd, 2000, with $C = 1.39$), respectively. In Figure 1 (lower panel), we also show the evolution of the atmospheric seeing during the observations. It can be clearly seen that there is no correlation with the blazar differential lightcurve. A seeing-variability correlation test was made for all sources in the sample as recommended by Cellone et al. (2000) and implemented, for example, by Clements & Carini (2001).

Complete lightcurves for all objects in the sample are published electronically as Figures 2.1 to 2.20.

In Figure 3 we present an histogram with the distribution of variability amplitudes Δm_V for all objects in the sample. The highest microvariations in a single night are about 0.5 mag. Most of the sources, however, present less violent changes.

In Figure 4 we show a similar histogram with the distribution of the microvariability timescales. These are the timescales presented by the largest amplitude variations occurred within a single night in variable sources, and are defined as $t_v = (1+z)^{-1} \Delta F / (dF/dt)$, where F is the flux density and the factor $(1+z)^{-1}$ is the cosmological correction. It can be seen that the shortest timescales are of ~ 1 hour. Two peaks in the histogram indicate that the preferred intranight timescales occur at 2-3 hours and 6-7

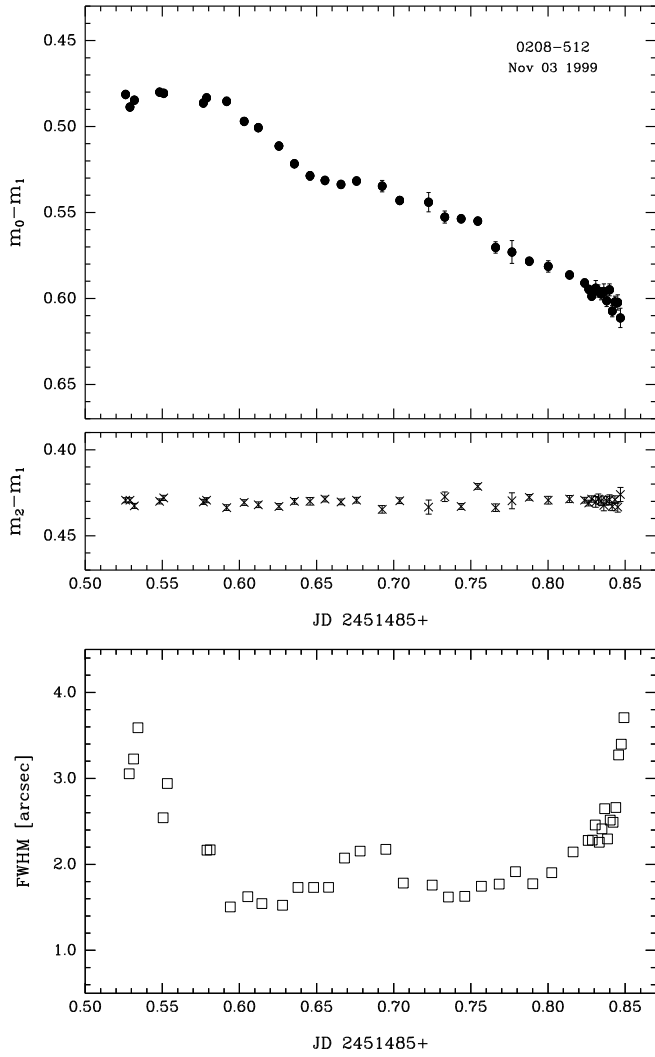


Fig. 1. Differential lightcurve for 0208–512 on the night of November 3rd, 1999, a typically variable blazar in the sample (filled circles). Comparison stellar lightcurve is also shown (crosses). In the lower panel we show the atmospheric seeing evolution for this night at CASLEO telescope (open squares). Notice the absence of correlation.

hours, although the second peak may be an artifact of the observational sampling interval, since most sources were followed during 6–7 hours per night. Figure 5 shows a plot of t_v vs. Δm_v , where it can be seen that the largest in-tranight fluctuations occur with timescales in the range 2 – 6 hours.

4. Duty cycle of EGRET blazars

Duty cycles for objects of a given class can be roughly estimated as (Romero et al. 1999):

$$DC = 100 \frac{\sum_{i=1}^n N_i (1/\Delta t_i)}{\sum_{i=1}^n (1/\Delta t_i)} \%, \quad (1)$$

where $\Delta t_i = \Delta t_{i,\text{obs}}(1+z)^{-1}$ is the duration (corrected by redshift) of the i -st observing session of a source of the

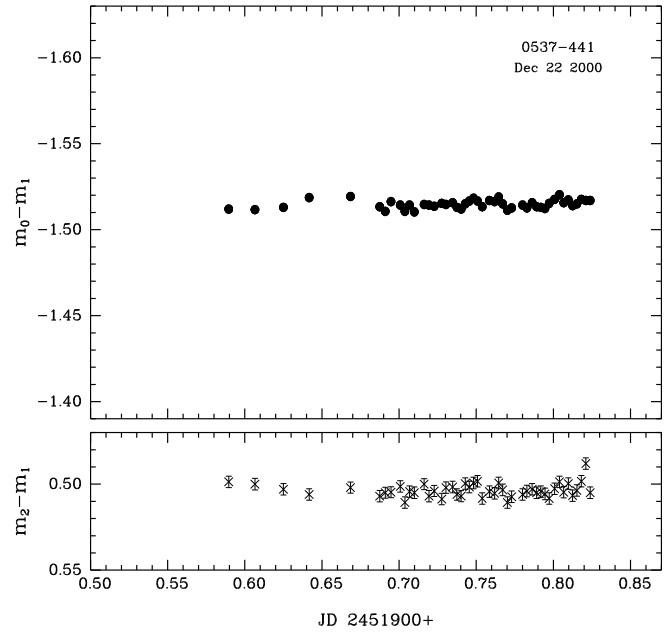


Fig. 2. Lightcurve for PKS 0537–441 on the night of December 22nd, 2000. The source was not variable this particular night. Comparison stellar lightcurve is also shown.

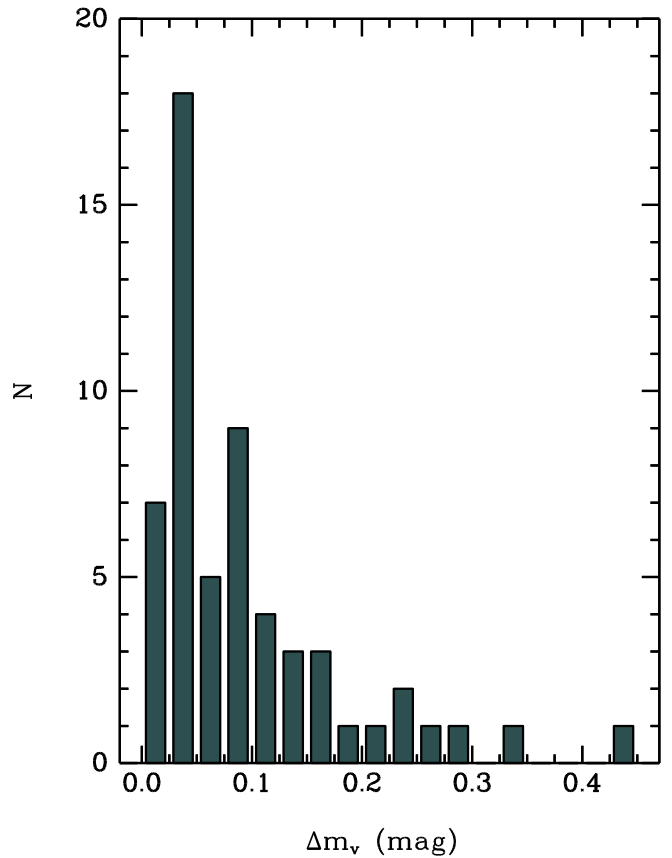


Fig. 3. Histogram with variability amplitudes for all objects in the sample.

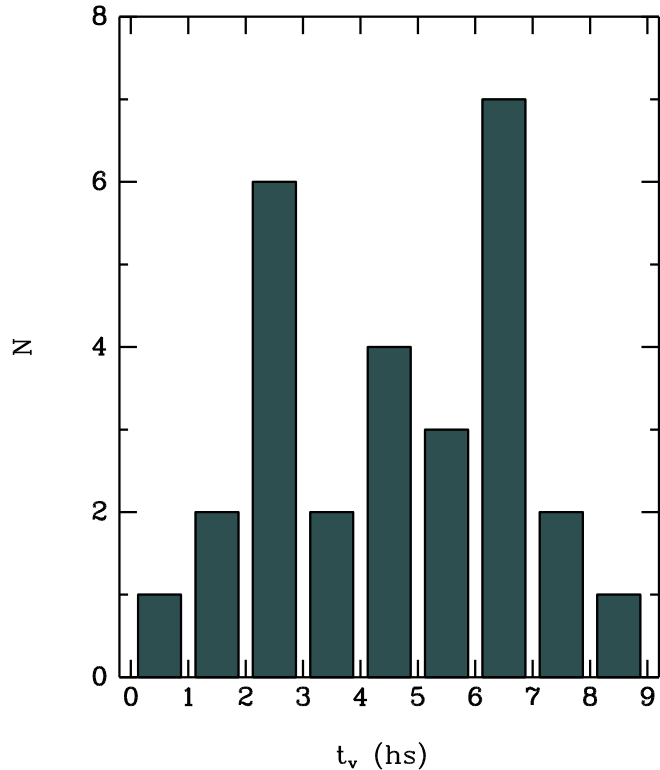


Fig. 4. Histogram with the microvariability timescales for variable objects in the sample.

class under study, and N_i equals 0 or 1 if the object was classified as NV or V during Δt_i , respectively. Using this formula, Romero et al. (1999) have estimated a DC of 71.5 % for RBLs and RLQs, of 61.9 % for radio-loud Seyfert 1 galaxies (RS1s), of 27.9 % for XBLs, and of only 2.7 % for radio-quiet QSOs. The class of the gamma-ray blazars detected by EGRET includes objects classified as RBLs, RLQs and XBLs. If we estimate, using Eq. (1), the DC for EGRET blazars as a class, we get a value of 48.8 %. This estimate is based on a sample of 20 EGRET blazars and 57 independent observing sessions. In Figure 6 we present a graphic comparison between the DC of different classes of AGNs. We also indicate the value obtained for the DC of EGRET blazars when longer timescales (internight: $\Delta t_i = 2$ consecutive sessions) are considered. In this case we get $DC = 67.7$ %, and we are closer to the values presented by the total class of flat-spectrum radio loud sources. The conclusion seems to be that EGRET blazars are more active at optical wavelengths on *internight* than on *intranight* timescales.

We emphasize that despite the time resolution of our observations is very high, in any case we have detected the kind of events reported by Xie et al. (1999, 2001, 2002) for some EGRET blazars of our sample. These authors claim detections of extreme events in objects included in our sample like 1253–055 (3C279), 1510–089, and AO 0235+164 over timescales of a few minutes. For instance, they report a variation of $\Delta V = 1.17$ mag within 40 minutes on May 22, 1996 for 1253–055 and of

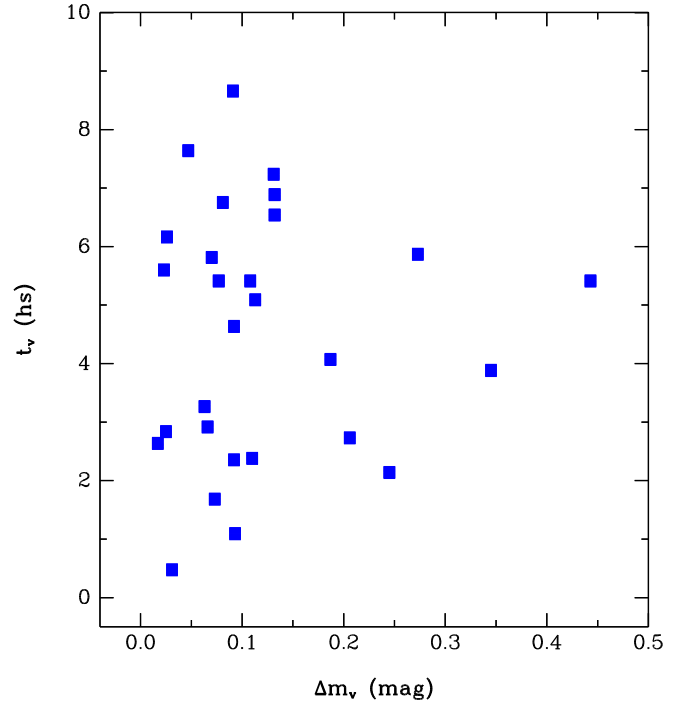


Fig. 5. Plot of the microvariability timescales vs. the variability amplitude for objects in the sample that are variable within a single night.

$\Delta V = 0.52$ mag within 10 minutes on January 17, 1999 for AO 0235+164. Our observations show no indication of microvariability in objects like 1510–089 and, indeed, strong variations in AO 0235+164, an object with $DC \sim 100$ %, but never over such extremely short timescales as reported by Xie et al. As communicated by Romero et al. (2000a), this latter source shows changes of $\Delta V \sim 0.5$ mag within a single night, but the well-resolved lightcurves we have obtained present no indication of large-amplitude changes on shorter (say less than 1 hour) timescales. It could be argued that these particular sources could undergo extreme behaviour from time to time and we have failed in its detection. But such a behaviour was not observed in any of the 20 sources of our sample of gamma-ray blazars. Since the minute-scale flares are claimed to be present in many of the objects in the sample of Xie et al., the probability that we would have observed none of them along 57 observing sessions is extremely low. The mean DC for minute-scale microvariations seems to be ~ 50 % (Xie et al. 2001), consequently the probability of finding zero of such microvariations in our entire campaign is $\sim 7 \times 10^{-18}$.

A more likely alternative is that the discrepancies between both works arise from different methods for error control. Xie et al. (1999, 2001, 2002) give no information on seeing fluctuations, aperture size adopted for the photometric analysis, or light pollution from the host. Recently, Cellone et al. (2000) have demonstrated that strong spurious variations in photometric observations of AGNs can occur even in the absence of significant variability of the field stars, when the AGN is embedded within

a detectable host galaxy. These effects, however, can be prevented through some simple techniques that we have applied in our study (see Section 2 and Cellone et al. 2000 for additional details).

In a recent paper, Dai et al. (2001) report to have also found large-amplitude magnitude variations on very short timescales, even after preventing against the effects of seeing induced light contamination from the host galaxy. However, a likely error source in their data analysis, as well as in those of Xie et al., lies in the fact that many of the standard stars they used for calibration purposes are significantly brighter than the corresponding AGN.

Remarkably, all the program objects reported to display fast, large amplitude variations in Xie et al.’s papers and in Dai et al. (2001), are those for which the magnitude difference AGN – standards is largest (from ~ 2.5 and up to ~ 5 mag, standards always brighter). Our comparison and control stars, instead, typically differ by only a few tenths of a magnitude from the corresponding AGN, with a couple of extreme cases reaching a ~ 1.5 mag difference. This ensures a correct matching of photometric and aperture centering errors between AGN and comparison-control stars. Let us mention that, because of their relatively high brightnesses, all the standard stars in the field of AO 0235+164 used by Xie et al. (2001) are saturated in most of our images. The same is true for 1510–089, for which Dai et al. (2001) report a 1.72 mag fading in 27 minutes followed by a 2.00 mag brightening in 13 minutes, with a variability parameter $C = 59.6$. Note, however, that comparison star 1 in Dai et al. (2001) is 5 magnitudes (i.e., 100 times in flux units) brighter than the AGN, while star 2 is ~ 3.3 mag brighter than the AGN [See Raiteri et al. (1998) for coordinates and a finding chart for these stars]. It is clear that, even with a high dynamic-range CCD, it is not possible to properly expose the AGN in order to achieve a sufficiently high signal-to-noise ratio without saturating the comparison star.

It is thus not surprising that Dai et al. (2001) have found such a high variability parameter C for 1510–089. In fact, a simple error analysis indicates that, with their observational setup, $C \simeq 17$ should be expected from Poissonian noise alone, without considering possible systematic errors from non-linearity or saturation, and even under excellent atmospheric conditions and supposing a fairly dark sky ($\mu_R = 21$ mag arcsec $^{-2}$). For a site with a sky 1.5 mag arcsec $^{-2}$ brighter, a slightly larger value ($C \simeq 19$) is obtained. Things get worse under non-photometric atmospheric conditions, when the (faint) AGN will be relatively more affected than the (bright) comparison star by the inevitable falloff in S/N ratio.

We conclude, contrary to previous claims, that the typical minimum timescale for microvariations of EGRET blazars is of \sim several hours (not tens of minutes) and that the duty cycle for optical microvariability in these objects peaks at timescales of $\sim 1-2$ days, in accordance with the short-term gamma-ray timescales observed in several objects (e.g., Hartman 1996; Hartman et al. 2001; Mukherjee

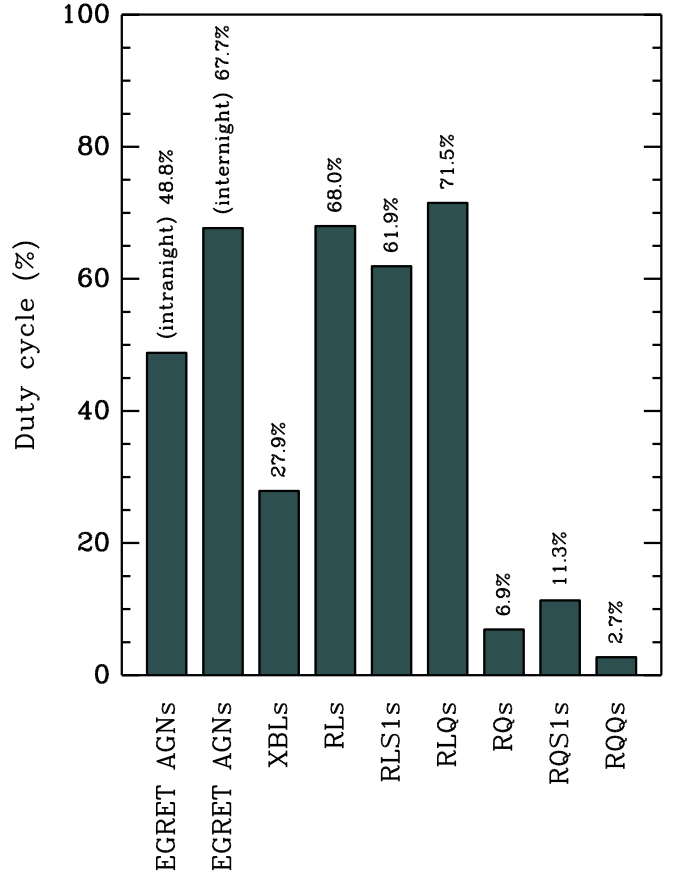


Fig. 6. Duty cycles for different types of AGNs, including EGRET blazars, at strictly intranight timescales. The duty cycle for EGRET blazars at longer timescales (2 days) is also shown for comparison. The group labeled as RQ includes both RQS1s and RQQs, whereas RL objects are both RBLs and RLQs.

2001). This result is important since it implies that the optical and gamma-ray emitting regions have similar sizes.

5. Discussion

Whereas the radio-to-UV continuum from blazars is usually interpreted as synchrotron emission from energetic leptons in a relativistic jet, the gamma-ray photons are thought to be the result of inverse Compton scattering of soft seed photon fields by the same leptonic population. The origin of these soft photons is not clear and different possibilities have been discussed in the literature, including external photon fields (accretion disk, broad line region) and the own synchrotron photons produced in the jet (the so-called synchrotron self-Compton model –SSC–). The reader can find the relevant references in the already cited paper by Hartman et al. (2001).

Gamma-ray blazars are known to vary their flux on timescales as short as 1 – 2 days according to EGRET intensive monitoring of a few selected sources like 3C279 and PKS 1406-076 (e.g., Wagner et al. 1995; Hartman et al. 2001). The shortest gamma-ray timescales are about 8

hs, as reported for 3C279 by Wehrle et al. (1998). These timescales are similar to the preferred timescales for optical microvariability in EGRET blazars according to our study. This seems to favor the idea that the optical and gamma-ray emission are co-spatial, with sizes typically in range $10^{15} - 10^{16}$ cm. Emission regions of such sizes are in accordance with the constraints imposed by pair creation processes (e.g., Blandford & Levinson 1995). However, from non-simultaneous observations the nature of the seed photons cannot be inferred. If simultaneous optical/gamma observations clearly reveal the existence of correlated microvariability with zero time lag, then SSC models would be favored. On the contrary, non-simultaneous but well correlated bursts could point out to external Compton models. In particular, an optical burst preceding the gamma-ray flare (as in Wagner et al. 1995) could be indicative of externally rescattered/reprocessed synchrotron radiation of the jet (Ghisellini & Madau 1996).

The fact that the minimum optical timescales for large microvariations are of at least of several hours seems to agree with the suggestion that in EGRET blazars the same population of relativistic particles is responsible for both the optical and gamma-ray variable emission. If the shortest optical timescales actually were of a few tens of minutes, as claimed by Xie et al., then the optically emitting region should be smaller than the Schwarzschild radius for objects like 3C279.

The most promising scenario to explain the production of both optical and gamma-ray flares in blazars is perhaps the so-called shock-in-jet model, where the increase in the flux density is the result of shocks formed due to velocity irregularities in the relativistic flow of the jet (e.g., Marscher & Gear 1985; Sikora et al. 2001). Particles in the shocked region cool through synchrotron radiation at optical wavelengths and through inverse Compton mechanism at gamma-ray energies. Future simultaneous optical/gamma-ray monitoring campaigns of blazars with high time resolution using instruments like the forthcoming GLAST satellite will help to solve the mystery of the origin of high-energy emission in these objects and will provide elements to constrain the models of nonthermal flares.

Acknowledgements. The authors acknowledge use of CCD and data acquisition system supported under US National Science Foundation grant AST-90-15827 to R.M. Rich. They are also very grateful to the CASLEO staff for their kind assistance during the observations. GER thanks the kind hospitality of the Max-Planck-Institut für Kernphysik at Heidelberg, where the final part of this work was done. This research was supported by CONICET (PIP 0430/98), ANPCT (PICT 03-04881) and Fundación Antorchas.

References

- Blandford, R. D., & Levinson, A. 1995, ApJ, 441, 79
 Cellone, S. A., Romero, G. E., & Combi, J. A. 2000, AJ, 119, 1534
 Clements, S. D., & Carini, M. T. 2001, AJ, 121, 90
 Dai, B. Z., Xie, G. Z., Li, K. H., et al. 2001, AJ, 122, 2901
 Fiorucci, M., Tosti, G., & Rizzi, N. 1998, PASP, 110, 105
 Ghisellini, G., & Madau, P. 1996, MNRAS, 280, 67
 Gopal-Krishna, Gupta, A. C, Sagar, R., et al. 2000, MNRAS, 314, 815
 Hartman, R. C. 1996, in ASP Conf. Ser. 110, Blazar Continuum Variability, eds. H. R. Miller, J. R. Webb, & J. C. Noble, 333
 Hartman, R. C., Bertsch, D. L., Bloom, S. D., et al. 1999, ApJS, 123, 79
 Hartman, R. C., Villata, M., Balonek, T. J., et al. 2001, ApJ, 558, 583
 Heidt, J., & Wagner, S. J. 1996, A&A, 305, 42
 Heidt, J., & Wagner, S. J. 1998, A&A, 229, 853
 Jang, M., & Miller, H. R. 1997, AJ, 114, 565
 Kraus, A., Quirrenbach, A., Lobanov, A. P., et al. 1999, A&A, 344, 807
 Landolt, A. U. 1992, AJ, 104, 340
 Mangalam, A. V., & Wiita, P. J. 1993, ApJ, 406, 420
 Marscher, A.P. & Gear, W. 1985, ApJ, 298, 114
 Mattox, J. R., Schachter, J., Molnar, L., et al. 1997, ApJ, 481, 95
 Miller, H. R., Carini, M. T., & Goodrich, B. 1989, Nature, 337, 627
 Mukherjee, R. 2001, in AIP Proc. 558, High Energy Gamma-Ray Astronomy, eds. F. A. Aharonian & H. J. Völk, 324
 Qian, S. J., Quirrenbach, A., Witzel, A., et al. 1991, A&A, 241, 15
 Qian, S. J., Kraus, A., Witzel, A., et al. 2000, A&A, 357, 84
 Qian, B., Tao, J., & Fan, J. H. 2000, PASJ, 52, 1075
 Qian, B., Tao, J., & Fan, J. H. 2002, AJ, 123, 678
 Racine, R. 1970, ApJ, 159, L99
 Raiteri, C. M., Villata, M., Lanteri, L., Cavallone, M., & Sobrito, G. 1998, A&AS, 130, 495
 Romero, G. E. 1995, Ap&SS, 234, 49
 Romero, G. E., Cellone, S. A., & Combi, J. A. 1999, A&AS, 135, 477
 Romero, G. E., Cellone, S. A., & Combi, J. A. 2000a, A&A, 360, L47
 Romero, G. E., Cellone, S. A., & Combi, J. A. 2000b, AJ, 120, 1192
 Sikora, M., Blazejowski, M., Begelman, M.C., & Moderski, R. 2001, ApJ, 554, 1
 Smith, P. S., Balonek, T. J., Heckert, P. A., Elston, R., & Schmidt, G. D. 1985, AJ, 90, 1184
 Wagner, S. J., Mattox, J. R., Hopp, U., et al. 1995, ApJ, 454, L97
 Wehrle, A. E., Pian, E., Urry, C.M., et al. 1998, ApJ, 497, 178
 Xie, G. Z., Li, K. H., Zhang, X., Bai, J. M., & Liu, W. W. 1999, ApJ, 522, 846
 Xie, G. Z., Li, K. H., Bai, J. M., et al. 2001, ApJ, 548, 200
 Xie, G. Z., Zhou, S. B., Dai, B. Z., et al. 2002, MNRAS, 329, 689

Table 2. Observational Results

Object	UT Date	q	σ mag	Δt h	Variable?	C	Δm_V mag	$\langle V \rangle$ mag
0208–512	11/03/99	3	0.003	7.75	V	18.01	0.131	15.65 ± 0.02
	11/04/99	2	0.002	7.61	V	2.60	0.023	15.61 ± 0.02
0235+164	11/03/99	3	0.014	6.65	V	10.10	0.273	17.09 ± 0.01
	11/04/99	2	0.012	6.57	V	6.10	0.245	17.47 ± 0.01
	11/05/99	3	0.012	6.93	V	8.92	0.345	17.32 ± 0.01
	11/06/99	2	0.007	6.68	V	4.37	0.110	17.89 ± 0.01
	11/07/99	1	0.009	6.58	V	14.34	0.443	17.02 ± 0.01
	11/08/99	4	0.009	2.26	V	2.75	0.092	17.27 ± 0.01
	12/22/00	2	0.007	7.20	V	3.30	0.070	17.32 ± 0.01
	12/24/00	2	0.008	3.21	V	7.89	0.206	17.11 ± 0.02
0521–365	12/17/98	1	0.005	6.41	V	3.32	0.063	15.03 ± 0.03
0537–441	12/22/97	1	0.002	5.70	V	9.45	0.073	16.79 ± 0.01
	12/23/97	1	0.003	6.10	V	7.00	0.066	16.69 ± 0.01
	12/16/98	3	0.005	6.90	V	4.55	0.077	16.11 ± 0.02
	12/17/98	1	0.003	7.00	V	13.65	0.113	16.26 ± 0.02
	12/18/98	1	0.002	6.80	V	2.82	0.026	16.34 ± 0.01
	12/19/98	4	0.004	3.20	V	3.10	0.047	16.25 ± 0.02
	12/20/98	2	0.002	5.50	NV	2.25	0.025	16.04 ± 0.02
	12/21/98	2	0.002	6.50	V	2.65	0.025	16.11 ± 0.02
	12/20/00	4	0.005	1.57	NV	0.51	0.008	14.30 ± 0.05
	12/21/00	1	0.002	7.04	NV	2.55	0.027	14.33 ± 0.04
	12/22/00	2	0.002	5.62	NV	1.39	0.012	14.33 ± 0.03
	12/23/00	1	0.002	4.99	V	2.91	0.017	14.31 ± 0.01
	12/24/00	2	0.002	6.92	V	3.60	0.031	14.22 ± 0.01
1226+023	04/08/00	1	0.005	7.60	NV	0.69	0.015	12.71 ± 0.02
	04/09/00	2	0.005	3.33	NV	1.16	0.030	12.67 ± 0.02
1229–021	04/11/00	1	0.008	8.10	NV	1.15	0.034	16.86 ± 0.01
	04/12/00	1	0.009	8.19	NV	1.19	0.046	16.86 ± 0.01
1243–072	04/08/00	1	0.020	7.52	NV	2.24	0.167	19.75 ± 0.03
	04/09/00	2	0.020	7.97	V	3.00	0.187	19.74 ± 0.03
1253–055	06/08/99	4	0.024	3.81	NV	0.80	0.095	17.06 ± 0.05
1331+170	04/10/00	4	0.005	3.26	NV	1.17	0.026	16.34 ± 0.04
1334–127	04/11/00	1	0.009	8.82	NV	2.31	0.080	16.99 ± 0.01
	04/12/00	1	0.009	8.44	V	2.67	0.081	17.16 ± 0.01
1424–418	06/04/99	4	0.023	5.99	NV	1.91	0.172	18.81 ± 0.03
	06/05/99	3	0.013	6.86	NV	1.86	0.081	18.85 ± 0.02
1510–089	04/29/98	3	0.004	3.74	NV	2.49	0.026	17.28 ± 0.02
	04/30/98	3	0.008	3.97	NV	1.45	0.042	17.26 ± 0.02
	06/06/99	4	0.009	7.23	NV	1.05	0.034	16.98 ± 0.03
	06/07/99	2	0.008	7.31	NV	1.27	0.042	16.97 ± 0.06
1606+106	07/23/01	1	0.005	4.59	NV	1.63	0.019	17.89 ± 0.02
	07/24/01	1	0.009	4.66	V	3.08	0.092	17.81 ± 0.02
1622–297	06/04/99	4	0.021	6.75	NV	2.11	0.171	18.38 ± 0.16
	06/05/99	3	0.010	7.47	V	3.21	0.132	18.34 ± 0.16
1741–038	06/06/99	4	0.025	7.92	NV	1.07	0.103	18.58 ± 0.03
	06/07/99	2	0.021	8.12	NV	1.73	0.151	18.57 ± 0.07
1933–400	07/23/01	1	0.008	9.05	NV	1.50	0.047	18.02 ± 0.02
	07/24/01	1	0.006	8.82	NV	2.28	0.071	18.00 ± 0.02
2022–077	07/25/01	1	0.010	6.94	V	4.12	0.132	17.66 ± 0.04
	07/26/01	1	0.005	6.39	V	4.89	0.091	17.06 ± 0.04
2155–304	07/27/97	3	0.002	7.00	NV	1.06	0.023	12.98 ± 0.02
	07/28/97	3	0.006	7.20	NV	0.73	0.027	12.98 ± 0.02
2230+114	07/23/01	1	0.004	5.74	NV	2.24	0.031	16.91 ± 0.02
	07/24/01	1	0.003	5.70	V	13.16	0.108	16.80 ± 0.02
	07/25/01	1	0.005	2.19	V	6.80	0.093	16.39 ± 0.01
2320–035	07/25/01	1	0.005	6.18	NV	1.90	0.036	16.61 ± 0.02
	07/26/01	1	0.007	2.64	NV	1.38	0.026	16.58 ± 0.02

Table 3. Comparison and control stars.

Id.	Comparison stars			Id.	Control stars		
	R.A. hs : min : s	Dec. ° : ' : "	V mag		R.A. hs : min : s	Dec. ° : ' : "	V mag
			0208−512				
C _{1,1}	02:10:32.9	-51:03:11	14.5	C _{2,1}	02:10:36.2	-50:59:31	14.6
C _{1,2}	02:10:39.4	-50:58:16	14.7	C _{2,2}	02:10:57.0	-51:01:52	15.7
C _{1,3}	02:10:53.3	-50:58:26	16.1	C _{2,3}	02:10:43.2	-51:03:25	16.2
			0235+164				
C _{1,1} ^a	02:38:38.4	16:38:19	16.8	C _{2,1}	02:38:38.5	16:40:07	17.4
			0521−365				
C _{1,1}	05:23:06.8	-36:24:58	14.7	C _{2,1}	05:22:40.4	-36:26:13	15.2
C _{1,2}	05:23:01.5	-36:25:01	16.5	C _{2,2}	05:22:49.8	-36:29:24	16.0
C _{1,3}	05:23:02.8	-36:27:43	16.6	C _{2,3}	05:22:53.6	-36:23:24	16.6
			0537−441				
C _{1,1}	05:38:55.7	-44:06:22	14.8	C _{2,1}	05:39:09.1	-44:03:25	14.0
C _{1,2}	05:39:06.7	-44:03:11	15.2	C _{2,2}	05:38:37.7	-44:03:25	14.5
C _{1,3}	05:38:29.9	-44:04:59	15.2	C _{2,3}	05:38:59.6	-44:03:14	14.6
			1226+023				
C _{1,1} ^b	12:29:08.4	02:00:20	12.7	C _{2,1} ^c	12:29:03.1	02:03:19	13.5
C _{1,2}	12:28:49.7	02:04:31	15.5	C _{2,2} ^d	12:29:02.9	02:02:17	14.9
			1229−021				
C _{1,1}	12:32:03.6	-02:21:57	17.2	C _{2,1}	12:32:10.8	-02:26:22	16.2
C _{1,2}	12:32:03.1	-02:26:05	17.3	C _{2,2}	12:32:09.1	-02:25:26	16.9
C _{1,3}	12:32:13.7	-02:24:54	17.8	C _{2,3}	12:32:15.4	-02:24:13	17.0
			1243−072				
C _{1,1}	12:46:13.0	-07:32:13	18.1	C _{2,1}	12:46:01.2	-07:32:04	18.6
C _{1,2}	12:46:07.7	-07:33:55	19.2	C _{2,2}	12:46:06.7	-07:28:40	19.0
C _{1,3}	12:46:11.0	-07:30:45	19.4	C _{2,3}	12:46:01.2	-07:29:16	19.3
			1253−055				
C _{1,1} ^e	12:56:26.6	-05:45:21	16.4	C _{2,1}	12:56:04.3	-05:51:15	16.7
C _{1,2}	12:56:04.1	-05:49:11	17.8	C _{2,2}	12:56:26.4	-05:48:46	18.2
			1331+170				
C _{1,1}	13:33:24.5	16:49:29	15.6	C _{2,1}	13:33:33.4	16:47:47	16.0
C _{1,2}	13:33:32.6	16:49:42	16.0	C _{2,2}	13:33:12.7	16:50:43	16.3
			1334−127				
C _{1,1}	13:37:34.6	-12:58:16	17.9	C _{2,1}	13:37:41.0	-12:56:35	17.4
C _{1,2}	13:37:48.0	-12:54:22	18.0	C _{2,2}	13:37:47.8	-12:56:53	17.6
			1424−418				
C _{1,1}	14:27:51.8	-42:06:18	18.4	C _{2,1}	14:27:58.6	-42:08:06	17.6
C _{1,2}	14:27:54.5	-42:05:38	18.5	C _{2,2}	14:27:48.0	-42:08:42	18.4
C _{1,3}	14:27:51.6	-42:05:42	19.0	C _{2,3}	14:27:54.5	-42:09:14	18.6
			1510−089				
C _{1,1}	15:12:53.0	-09:05:41	16.7	C _{2,1}	15:12:41.8	-09:05:51	17.0
C _{1,2}	15:13:00.0	-09:05:42	17.5	C _{2,2}	15:12:51.4	-09:08:00	17.4
			1606+106				
C _{1,1}	16:08:51.8	10:31:14	17.4	C _{2,1}	16:08:48.0	10:27:27	17.4
C _{1,2}	16:08:46.3	10:30:09	18.4	C _{2,2}	16:08:51.8	10:32:40	17.6
C _{1,3}	16:08:48.5	10:29:01	18.7	C _{2,3}	16:08:48.5	10:31:57	17.7

Table 3. *Continued.*

Id.	Comparison stars		<i>V</i> mag	Id.	Control stars		<i>V</i> mag
	R.A. hs : min : s	Dec. ° : ' : ''			R.A. hs : min : s	Dec. ° : ' : ''	
1622–297							
C _{1,1}	16:28:46.2	-29:51:53	18.2	C _{2,1}	16:25:19.2	-29:52:22	18.2
C _{1,2}	16:24:56.9	-29:51:02	18.3	C _{2,2}	16:30:21.6	-29:51:53	18.3
C _{1,3}	16:25:53.4	-29:52:43	18.4	C _{2,3}	16:25:22.8	-29:51:18	18.5
1741–038							
C _{1,1}	17:43:49.0	-03:50:12	18.0	C _{2,1}	17:44:01.4	-03:49:22	18.0
C _{1,2}	17:43:55.4	-03:47:48	18.2	C _{2,2}	17:44:01.9	-03:50:23	18.5
1933–400							
C _{1,1}	19:37:10.3	-39:55:44	17.7	C _{2,1}	19:37:24.7	-39:54:29	17.9
C _{1,2}	19:37:20.6	-39:59:02	18.0	C _{2,2}	19:37:25.4	-39:59:53	18.1
C _{1,3}	19:37:20.9	-39:57:40	18.2	C _{2,3}	19:37:21.8	-39:56:35	18.3
2022–077							
C _{1,1}	20:25:52.6	-07:35:27	17.0	C _{2,1}	20:25:44.2	-07:37:57	17.2
C _{1,2}	20:25:48.5	-07:32:55	17.6	C _{2,2}	20:25:49.4	-07:35:01	17.6
C _{1,3}	20:25:43.7	-07:39:38	18.0	C _{2,3}	20:25:45.1	-07:37:20	18.0
2155–304							
C _{1,1}	21:58:43.7	-30:17:17	14.1	C _{2,1}	21:58:38.4	-30:13:05	15.8
C _{1,2}	21:58:35.8	-30:13:34	14.9	C _{2,2}	21:58:43.9	-30:16:34	16.1
C _{1,3}	21:58:57.8	-30:13:26	15.4	C _{2,3}	21:59:01.7	-30:14:56	16.4
2230+114							
C _{1,1}	22:32:27.6	11:42:40	16.0	C _{2,1}	22:32:32.9	11:42:45	16.3
C _{1,2}	22:32:31.7	11:42:22	16.8	C _{2,2}	22:32:45.8	11:42:01	17.1
C _{1,3}	22:32:30.2	11:42:35	17.2	C _{2,3}	22:32:48.5	11:44:44	17.2
2320–035							
C _{1,1}	23:23:39.6	-03:18:58	15.9	C _{2,1}	23:23:29.0	-03:19:08	16.3
C _{1,2}	23:23:25.9	-03:19:34	17.0	C _{2,2}	23:23:35.5	-03:14:47	17.1
C _{1,3}	23:23:33.8	-03:15:33	17.3	C _{2,3}	23:23:39.6	-03:15:07	17.5

a: Star 8 in Smith et al. 1985*b*: Star E in Fiorucci et al. 1998*c*: Star G in Fiorucci et al. 1998*d*: Star B' in Fiorucci et al. 1998*e*: Star 3 in Raiteri et al. 1998

This figure "fig2.01.jpg" is available in "jpg" format from:

<http://arxiv.org/ps/astro-ph/0205311v1>

This figure "fig2.01.png" is available in "png" format from:

<http://arxiv.org/ps/astro-ph/0205311v1>

This figure "fig2.02.jpg" is available in "jpg" format from:

<http://arxiv.org/ps/astro-ph/0205311v1>

This figure "fig2.03.jpg" is available in "jpg" format from:

<http://arxiv.org/ps/astro-ph/0205311v1>

This figure "fig2.04.jpg" is available in "jpg" format from:

<http://arxiv.org/ps/astro-ph/0205311v1>

This figure "fig2.05.jpg" is available in "jpg" format from:

<http://arxiv.org/ps/astro-ph/0205311v1>

This figure "fig2.06.jpg" is available in "jpg" format from:

<http://arxiv.org/ps/astro-ph/0205311v1>

This figure "fig2.07.jpg" is available in "jpg" format from:

<http://arxiv.org/ps/astro-ph/0205311v1>

This figure "fig2.08.jpg" is available in "jpg" format from:

<http://arxiv.org/ps/astro-ph/0205311v1>

This figure "fig2.09.jpg" is available in "jpg" format from:

<http://arxiv.org/ps/astro-ph/0205311v1>

This figure "fig2.10.jpg" is available in "jpg" format from:

<http://arxiv.org/ps/astro-ph/0205311v1>

This figure "fig2.11.jpg" is available in "jpg" format from:

<http://arxiv.org/ps/astro-ph/0205311v1>

This figure "fig2.12.jpg" is available in "jpg" format from:

<http://arxiv.org/ps/astro-ph/0205311v1>

This figure "fig2.13.jpg" is available in "jpg" format from:

<http://arxiv.org/ps/astro-ph/0205311v1>

This figure "fig2.14.jpg" is available in "jpg" format from:

<http://arxiv.org/ps/astro-ph/0205311v1>

This figure "fig2.15.jpg" is available in "jpg" format from:

<http://arxiv.org/ps/astro-ph/0205311v1>

This figure "fig2.16.jpg" is available in "jpg" format from:

<http://arxiv.org/ps/astro-ph/0205311v1>

This figure "fig2.17.jpg" is available in "jpg" format from:

<http://arxiv.org/ps/astro-ph/0205311v1>

This figure "fig2.18.jpg" is available in "jpg" format from:

<http://arxiv.org/ps/astro-ph/0205311v1>

This figure "fig2.19.jpg" is available in "jpg" format from:

<http://arxiv.org/ps/astro-ph/0205311v1>

This figure "fig2.20.jpg" is available in "jpg" format from:

<http://arxiv.org/ps/astro-ph/0205311v1>